PNAS RESEARCH ARTICLE | SYSTEMS BIOLOGY

Dynamic gene expression and growth underlie cell-to-cell heterogeneity in *Escherichia coli* stress response

Nadia M. V. Sampaio[a,b,1,2], Caroline M. Blassick[a,b,1], Virgile Andreani[a,b], Jean-Baptiste Lugagne[a,b], and Mary J. Dunlop[a,b,3]

Edited by James Collins, Massachusetts Institute of Technology, Cambridge, MA; received August 14, 2021; accepted February 23, 2022

Cell-to-cell heterogeneity in gene expression and growth can have critical functional consequences, such as determining whether individual bacteria survive or die following stress. Although phenotypic variability is well documented, the dynamics that underlie it are often unknown. This information is important because dramatically different outcomes can arise from gradual versus rapid changes in expression and growth. Using single-cell time-lapse microscopy, we measured the temporal expression of a suite of stress-response reporters in *Escherichia coli*, while simultaneously monitoring growth rate. In conditions without stress, we found several examples of pulsatile expression. Single-cell growth rates were often anticorrelated with reporter levels, with changes in growth preceding changes in expression. These dynamics have functional consequences, which we demonstrate by measuring survival after challenging cells with the antibiotic ciprofloxacin. Our results suggest that fluctuations in both gene expression and growth dynamics in stress-response networks have direct consequences on survival.

single cell | dynamics | growth | stress response

Significance

Individual bacteria that share identical genomes and growth environments can display substantial cell-to-cell differences in expression of stress-response genes and single-cell growth rates. This phenotypic heterogeneity can impact the survival of single cells facing sudden stress. However, the windows of time that cells spend in vulnerable or tolerant states are often unknown. We quantify the temporal expression of a suite of stress-response reporters, while simultaneously monitoring growth. We observe pulsatile expression across genes with a range of stress-response functions, finding that single-cell growth rates are often anticorrelated with reporter levels. These dynamic phenotypic differences have a concrete link to function, in which individual cells undergoing a pulse of elevated expression and slow growth are predisposed to survive antibiotic exposure.

Even under otherwise constant environmental conditions, genetically identical cells can display substantial phenotypic heterogeneity, resulting from differences in gene expression and growth rate from cell to cell (1–4). Phenotypic heterogeneity can, in principle, arise from slow changes within the population where individual cells have different expression levels or growth rates but maintain their state over many cell cycles. Alternatively, fast dynamics with rapid fluctuations could produce equivalent distributions. The distinction between these alternatives is significant because the timescale over which expression or growth differences persist can ultimately determine if they have functional consequences or are simply short-lived random variations that are filtered before impacting cellular outcomes. Although phenotypic heterogeneity is well-documented, the timescales underlying the variation and their ultimate impact on function are often less clear.

We focused on stress-response genes in *Escherichia coli* to study the dynamics of expression and growth in single cells. Genes involved in adaptation to stress are among the noisiest genome-wide (3, 5). Studies on individual pathways have revealed specific examples in which heterogeneous expression of stress-response genes can allow subpopulations of cells to survive sudden environmental stress, such as transient exposure to antimicrobial drugs, oxidative stress, and acid stress (6–9). Recent studies also indicate that heterogeneity in the expression of genes involved in DNA repair can lead to variability in mutation rates, contributing to microbial evolution (10–12). Notably, this diversity exists even in the absence of stressors. Although selected studies have begun to reveal examples of how cell-to-cell phenotypic variation can provide important functional capabilities to cell populations, examples of direct links are relatively sparse compared to reports quantifying phenotypic heterogeneity. This motivated our focus on stress-response pathways because the effect of the genes involved can be directly assessed by quantifying outcomes like cell survival versus death following stress.

In addition to measurements at a single time point, long-term monitoring of gene expression has begun to uncover examples of rich dynamics in key stress-response proteins (13). For example, self-cleavage of the regulator LexA produces spontaneous pulses in the SOS response network (14). Further, dynamic activity of transcription factors can propagate to downstream genes, with direct consequences for stress tolerance. For instance, pulsatile expression of the transcription factor ComK enables *Bacillus subtilis* cells to enter a transient competent state (15, 16). In *E. coli*, heterogeneous expression of RpoS, a key regulator of general stress response, originates from pulses of activation that are inversely correlated with growth, allowing cells to survive oxidative stress (8). Additionally, Kim et al. demonstrated that genes in the flagellar synthesis network, a process with a pivotal role in microbial pathogenicity, are expressed with different pulsing programs that allow cells to switch between flagellar phenotypes (17).

Author contributions: N.M.V.S. and M.J.D. designed research; N.M.V.S., C.M.B., and V.A. performed research; J.-B.L. contributed new reagents/analytic tools; C.M.B., V.A., and M.J.D. analyzed data; and N.M.V.S. and M.J.D. wrote the paper.

The authors declare no competing interest.

This article is a PNAS Direct Submission.

[1]N.M.V.S. and C.M.B. contributed equally to this work.

[2]Present address: Brazilian Biorenewables National Laboratory, Brazilian Center for Research in Energy and Materials, Campinas, 13083-100 São Paulo, Brazil.

[3]To whom correspondence may be addressed. Email: mjdunlop@bu.edu.

This article contains supporting information online at http://www.pnas.org/lookup/suppl/doi:10.1073/pnas.2115032119/-/DCSupplemental.

Published March 28, 2022.

Collectively, these studies demonstrate that the temporal dynamics of gene expression play an important role in the regulation of stress-response networks.

Growth rate fluctuations have also been observed in single cells across many bacterial species (2, 8, 18–20). They can arise due to temporal variation in the expression of metabolic enzymes (2, 21), the expression of burdensome proteins (12), and due to regulatory effects such as feedback involved in cell-size control (19). These single-cell differences in growth rate can play a functional role in stress tolerance. For example, Narula et al. demonstrated that the growth rate of *B. subtilis* under starvation conditions can determine whether individual cells differentiate into spores or remain vegetative (22). Single-cell growth rates also play a protective role, for example correlating with differential antibiotic susceptibility in mycobacteria (23) and *E. coli* (7, 24).

Understanding the timescales associated with gene expression dynamics and growth can provide critical insights into the strategies that cells use to hedge against environmental uncertainty. In this study, we characterize the prevalence and dynamic properties of cell-to-cell phenotypic variation in different branches of the stress-response network in *E. coli*. Using time-lapse microscopy, we monitored the activity of key stress-response genes, as well as genes involved in biosynthesis and metabolism, in single *E. coli* cells under precisely controlled, unstressed conditions. Our results reveal several examples of genes that exhibit pulses of gene expression. Furthermore, properties of the dynamics, such as the frequency or amplitude of pulsing, are unique to each gene. Interestingly, fluctuations in the expression of genes frequently occur following variations in growth rate. Dilution due to cell growth plays an important role in driving these fluctuations, but the precise relationship between growth and expression differs between the genes. Finally, we show that coincident up-regulation of stress-response genes and reduced growth rate favors tolerance to lethal antibiotic exposure. Together, this work reveals that nontrivial gene expression dynamics are common, even in otherwise constant conditions, and that these dynamic patterns of gene expression and growth can have critical consequences for cell survival.

Results

Single-Cell Measurements of Phenotypic Heterogeneity. We began by characterizing heterogeneity in the expression of genes with a diverse range of functions (*SI Appendix*, Table S1). These include genes involved in acid resistance (*gadW*, *gadX*, and *phoP*), multidrug resistance (*evgA*, *marA*, and *rob*), heat shock (*rpoH*), oxidative stress response (*oxyR*), SOS response (*dinB*, *recA*, and *sulA*), and general stress response (*bolA*), in addition to genes involved in biosynthesis and metabolism (*araC*, *metJ*, and *purA*).

To measure heterogeneity in the expression from each promoter at the single-cell level, we used strains containing transcriptional reporters where the promoter sequence of interest is fused to the coding sequence of a fluorescent protein. We grew independent bulk cultures of each strain to exponential phase and measured heterogeneity across cells in the population using fluorescence microscopy for single cells on agarose pads. Cell-to-cell differences in gene expression resulted in different distributions of reporter levels for each gene (Fig. 1*A* and *SI Appendix*, Fig. S1). Measurements of the reporters revealed many instances of wide distributions, indicative of a broad range of expression levels across cells within a population. Distributions tended to skew to the right of the mean (skew > 0) due to the presence of highly expressing cells.

However, measures of static distributions do not reveal the underlying dynamics that generate them, prompting the question: Do these distributions stem from long-lived fixed subpopulations with slow dynamics or from conditions with fast dynamics where individual cells transition between different expression levels over time (Fig. 1*B*)? The significance of this question is particularly pertinent in the context of stress-response networks, where the timescales over which individual genes are active may have concrete implications for tolerance levels. For instance, if a transcription factor that activates genes involved in stress response exhibits short pulses in expression, these pulses might be insufficient to turn on expression of downstream genes, while more sustained expression could. Further, single-cell growth rates can impact survival, and thus the interplay between expression and growth may be significant for determining tolerance.

Pulsatile Gene Expression Can Underlie Cell-to-Cell Heterogeneity. Thus, we next aimed to quantify the temporal dynamics underlying the distributions of gene expression and growth. We measured expression in cell lineages over many generations using a "mother-machine" microfluidic device (25) and time-lapse fluorescence microscopy. In this device, "mother" cells are trapped at the top of one-ended chambers and maintained indefinitely in exponential phase through the addition of fresh media, allowing for multihour imaging of cell lineages. We used this to monitor gene expression in tens to hundreds of independent cell lineages for each reporter for at least 15 h. To quantify gene expression over time, we used our deep learning-based cell segmentation and tracking algorithm (26) to extract single-cell resolution data from the mother cell and its progeny.

We observed heterogeneity in gene expression for cells growing in these precisely controlled conditions, which was consistent with measurements acquired from bulk culture snapshots (*SI Appendix*, Fig. S2). Further, our measurements of fluorescence correlate well with independent measurements from previous studies (*SI Appendix*, Fig. S3 and Table S2). Long-term monitoring of expression revealed a diversity of phenotypes, with some genes that fluctuated at a low level, likely due to variation in copy number in the reporter plasmid and inherent stochasticity in gene expression, while others were highly dynamic in their expression (Fig. 1 *C–E* and *SI Appendix*, Fig. S4). We observed that variability within a distribution often arose from pulsatile dynamics, with single cells transitioning smoothly between different expression states. These results join other recent single-cell studies showing transcriptional pulses in expression in the absence of stress (8, 14, 17).

We found that the timescales of these fluctuations were specific to each gene, and the pulses themselves ranged in intensity. For instance, *gadX*, which encodes a transcription factor that regulates ∼34 genes in the acid-resistance system, exhibits pulses of high amplitude and duration that persist well beyond the cell-cycle length, as visible in multigeneration patterns of gene expression (Fig. 1*C* and Movie S1). In contrast, *recA*, which plays a central role in the processes of homologous recombination and SOS response, showed large-amplitude pulses, but with shorter durations (Fig. 1*D* and Movie S2). Yet others, like *araC*, which encodes a transcription factor that regulates arabinose catabolism and transport, were more muted in their changes and exhibited only mild, low-amplitude fluctuations (Fig. 1*E* and Movie S3).

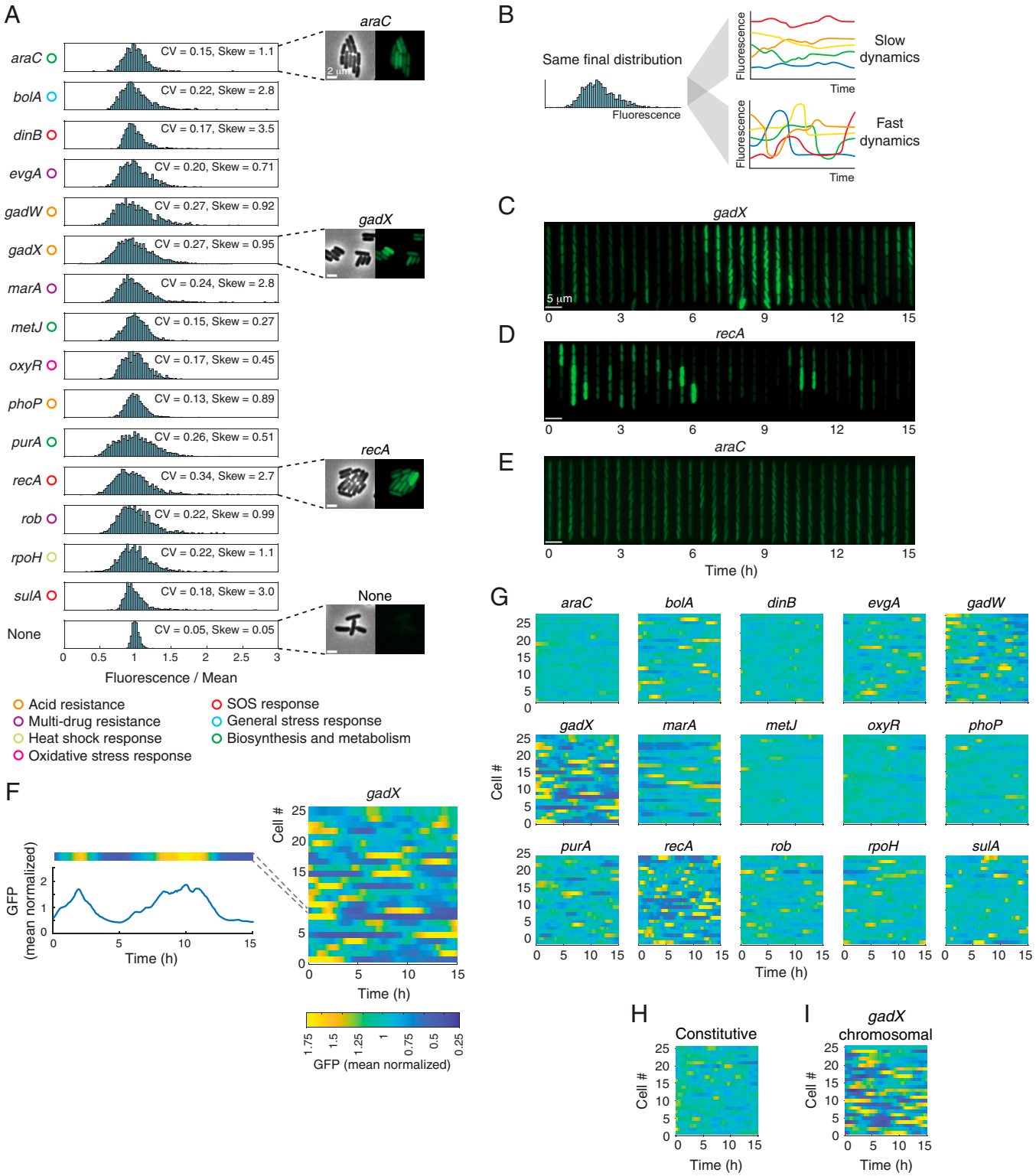

Fig. 1. Cell-to-cell heterogeneity and temporal dynamics of gene expression. (*A*) Histograms of fluorescence values show cell-to-cell variation. Values are presented normalized relative to their means to allow for comparison across reporters. The same data without normalization are shown in *SI Appendix*, Fig. S1. Corresponding coefficient of variation (CV) values obtained from snapshot images of cells grown in bulk cultures are listed in the figure. The skewness (skew) of the distribution, which is positive for distributions that are right-skewed, is also listed. (*Insets*) Phase contrast and fluorescence images for representative strains. Functional classes are listed for each gene. (Scale bar, 2 µm.) (*B*) Schematic representation of fluorescence signal over time originating from single cells with slow or fast dynamics of gene expression that result in identical fluorescence distributions for the final timepoint. (*C–E*) Representative kymographs of cells containing transcriptional fluorescent reporters for (*C*) *gadX*, (*D*) *recA*, and (E) *araC*. In all cases, fluorescence values are normalized to the mean to allow comparisons across the reporters. (Scale bars, 5 µm.) Corresponding phase contrast images and distributions of cell lengths are shown in *SI Appendix*, Fig. S4. (*F*) Single-cell measurements of GFP expression over time for the *gadX* reporter. Colored heat maps summarize the time-series data. (*G*) Heat maps summarizing the temporal dynamics of gene expression for all reporters. (*H*) Constitutive reporter heat map. (*I*) Chromosomally integrated *gadX* reporter heat map. In *F–I*, data from 25 cells are shown; however, this represents a subset of the time-series data. Color scale and normalization approach in *F* applies to all heat-map data.

Surveying 15 reporters, we observed a wide range of temporal gene expression profiles (Fig. 1 *F* and *G*). Despite the marked differences in temporal gene expression, cell length distributions were similar for strains harboring these different reporters (*SI Appendix*, Fig. S5*A*). We also measured correlations between fluorescence and cell length for all the reporters (*SI Appendix*, Fig. S5 *B* and *C*). These signals were not strongly correlated for most of the reporters. However, we did observe positive correlations between expression of *recA* and *sulA* and cell length. This result is expected, because these genes play a key role in the SOS response, which is known to induce cell filamentation (27–29). Even in unstressed conditions, we find that a small subset of cells exist in a state with high gene expression and corresponding elongated cell morphology. To rule out the possibility that the mother-machine architecture was introducing spurious relationships between growth rate and cell size or position within the chamber, we verified that growth rates were independent of both cell length and chamber position, indicating that the growth rate of mother cells is representative of all cells within the chambers (*SI Appendix*, Fig. S6). In all cases, the mean fluorescence levels were consistent across the duration of the experiments despite the fluctuations in gene expression at the single-cell level (*SI Appendix*, Fig. S7). Importantly, the dynamic activity observed for many reporters occurred under constant growth conditions, where parameters such as pH, temperature, and growth medium do not fluctuate.

As a control, we also included a plasmid-based constitutive reporter to quantify the baseline level of fluctuations expected from variation in plasmid copy number (Fig. 1*H*). The constitutive reporter exhibits mild changes in expression but does not reach the level of variation we observed in reporters like *gadX* and *recA*. As an additional control, we also chromosomally integrated the *gadX* reporter and confirmed that pulses in gene expression in cells containing the plasmid and chromosomally integrated versions of the reporters were comparable (Fig. 1*I*). Low expression levels prevented us from conducting all experiments using chromosomal reporters; however, the constitutive reporter serves as a control to establish baseline effects that are plasmid-based rather than specific to the stress-response reporters.

Properties of Temporal Expression Vary across the Reporters. Next, we defined several metrics across which to assess dynamic behavior. We selected properties related to pulses including their frequency, duration, and amplitude (Fig. 2*A*). Pulse frequencies were broadly distributed, ranging from examples that exceed 0.25 pulses per hour (one pulse every 4 h) for *recA* to much less frequent conditions where our peak-finding algorithm rarely identified pulses (Fig. 2*B*). Pulse durations typically ranged from 0 to 4 h and showed instances of precision (e.g., *recA* and *sulA*) in addition to examples with widely variable durations (e.g., *bolA*, *evgA*, and *rpoH*). Pulse amplitudes were predominantly small, with average amplitudes around 75% of the mean, or 0.75×, but there were notable instances where the distributions had long tails such that amplitudes extended well above this for a subset of the pulses. For example, *gadX* and *recA* exhibit pulses that significantly deviate from the mean. None of the pulse properties analyzed displayed a strong correlation with the mean expression of the reporters (*SI Appendix*, Fig. S8). To alleviate the potential concern that these relationships were a result of the specific method by which we identified pulses, we repeated the calculations under a range of different peak determination thresholds and found that our results were not sensitive to the precise threshold definition, provided the threshold was set high enough to exclude most fluctuations in the constitutive reporter control (*SI Appendix*, Fig. S9).

We next asked what characteristic timescales the gene expression dynamics exhibited by calculating the autocorrelation of the fluorescence signal. In all cases, we observed monotonically decreasing average autocorrelation curves (*SI Appendix*, Fig. S10). We calculated the half-life associated with the autocorrelation curve for each gene (Fig. 2 *C* and *D*). If the fluorescent reporter levels decrease solely due to dilution resulting from growth and division, the half-life will equal the cell division time. Longer half-lives can indicate the presence of memory, for example due to regulatory networks that cause signals to persist. We found that half-lives were always greater than or equal to the cell division time, consistent with the use of stable fluorescent reporters (Fig. 2*D*). Notably, we observed cases where the average exceeded the cell division time by two- to threefold, potentially indicative of memory within the network. We verified that these calculations performed on data from mother cells were consistent with correlations within the lineage tree. Indeed, tracking fluorescence signals from mother to daughter to granddaughter cells revealed a strong positive correlation that persisted across multiple generations (*SI Appendix*, Fig. S11).

RpoS Levels Influence *gadX* Pulsing Dynamics. One question that our results provoke is why some of the reporters exhibit pulsatile expression. We began by examining this in more detail for the case of the *gadX* reporter, which exhibited frequent pulses of high amplitude and duration. RpoS plays a role in *gadX* regulation and has been shown to exhibit pulsatile dynamics during exponential growth (8, 30, 31). Thus, we hypothesized that fluctuations in cellular RpoS levels during exponential growth could be underlying *gadX* pulsing. We used the same *gadX* reporter and compared expression in wild-type and Δ*rpoS* strains. Deletion of *rpoS* reduced *gadX* expression, and fluctuations in *gadX* expression became significantly less noticeable (Fig. 2*E* and *SI Appendix*, Fig. S12). We found that the frequency, duration, and amplitude of *gadX* pulses in the Δ*rpoS* cells were all reduced relative to the characteristic profile of wild-type cells (Fig. 2*F*), demonstrating the impact of RpoS on *gadX* pulsing dynamics. Experiments with the constitutive control show similar expression dynamics in both wild-type and Δ*rpoS* backgrounds, consistent with the lack of RpoS regulation of this reporter (Fig. 2 *G* and *H*).

To investigate whether RpoS modulates the dynamics of its different target genes in a standardized fashion, we also monitored the expression dynamics of two other RpoS-regulated reporters from our library, *evgA* and *gadW*, by comparing expression in the wild-type and Δ*rpoS* backgrounds (*SI Appendix*, Fig. S13). The overall dynamics of both reporters were altered in the Δ*rpoS* strain in comparison to wild type, confirming that RpoS has an important role in modulating the expression of its target genes during exponential phase. However, the impact of *rpoS* deletion on pulse metrics appears to be specific to each gene. These results suggest that RpoS modulation impacts expression dynamics, but its precise influence is gene-dependent.

For some of the reporters we used, the mechanism leading to pulsing dynamics has been revealed through prior studies. For example, pulsing dynamics for genes involved in SOS response, like *recA* and *sulA*, has been shown to originate from fluctuations in the availability of their common negative regulator LexA (14). Thus, fluctuations in master regulators of gene expression might be a common mechanism leading to heterogeneous expression of downstream genes.

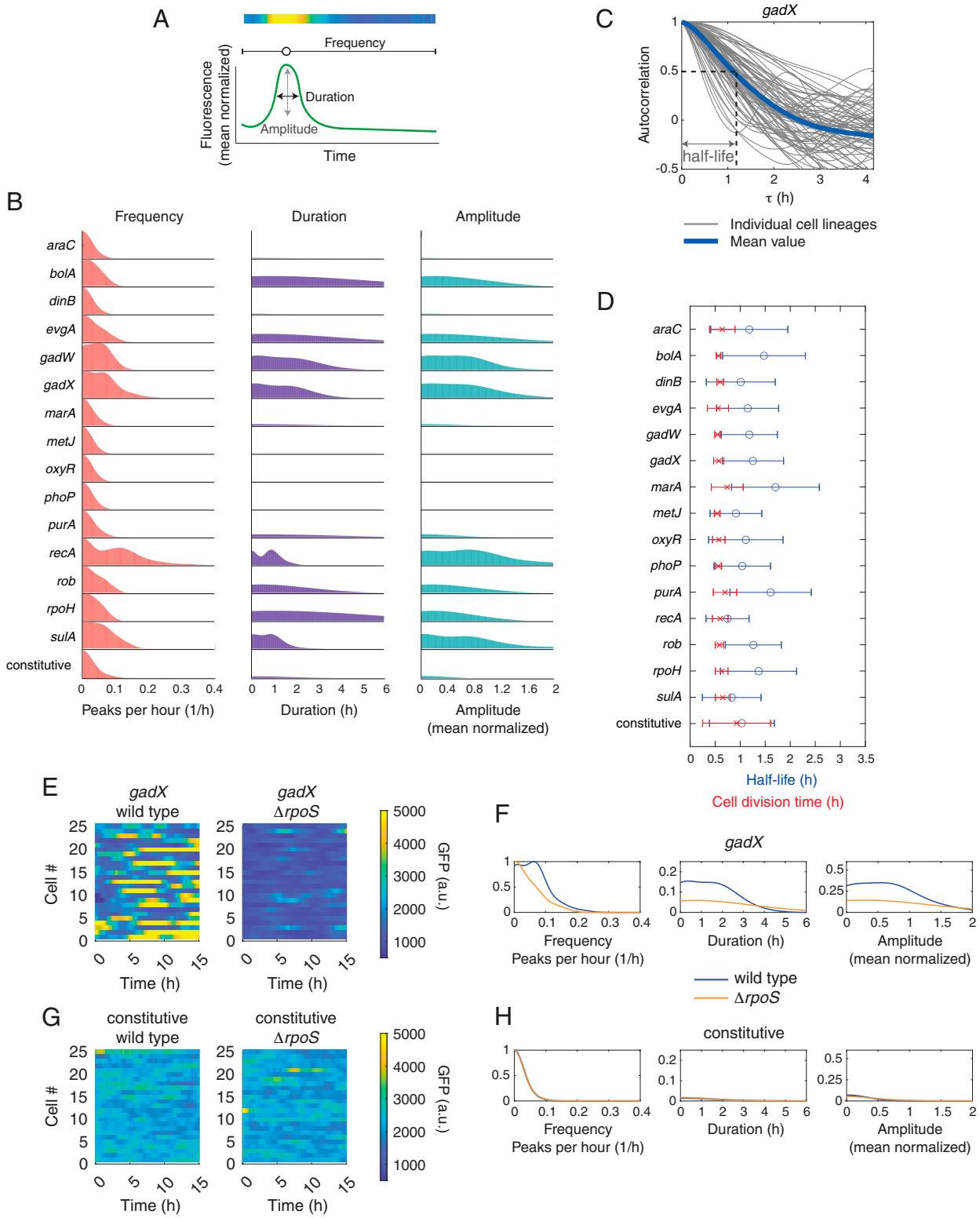

Fig. 2. Pulsing dynamics vary across the reporters. (*A*) Schematic representation of pulse characteristics. (*B*) Distributions of pulse frequency, duration, and amplitude for all reporters. Note that typical movie durations are 15 to 20 h (*SI Appendix*, Table S3); thus, we are limited in our ability to measure very low frequencies accurately (1/15 = 0.067). Duration and amplitude histograms are normalized such that the maximal height corresponds to the fraction of lineages with at least one pulse. (*C*) Autocorrelation of the fluorescence signal for independent cell lineages with the *gadX* reporter. Half-life is defined as the value of the time shift τ when the mean of the autocorrelation curve crosses 0.5. (*D*) Cell division time and half-life for each of the reporters. Error bars show SD around the mean. For the autocorrelation half-life calculations, half-lives are calculated using data from single cells, then mean and SD are calculated over these single-cell values. (*E*) Heat maps summarizing single-cell measurements of GFP over time for the *gadX* reporter in wild-type and Δ*rpoS* cells. Identical reporters are used in both strains, and thus the unnormalized data can be compared directly. (*F*) Frequency, duration, and amplitude distributions for the *gadX* reporter in the wild-type and Δ*rpoS* backgrounds. (*G*) GFP expression for the constitutive reporter in wild-type and Δ*rpoS* cells. Identical reporters are used in both strains, and thus the unnormalized data can be compared directly. (*H*) Frequency, duration, and amplitude distributions for the constitutive reporter in the wild-type and Δ*rpoS* backgrounds.

Pulsatile Expression Dynamics and Growth. We next asked whether growth rate contributes to the observed variability in expression levels. While the growth rate of individual *E. coli* cells shows long-term stability during replicative aging (25), it can exhibit noisy temporal behavior (2, 8, 19). We sought to quantify how temporal fluctuations in growth rate correlate with gene expression. Patange et al. demonstrated that growth rates fluctuate, with periods of slow growth that last for several generations and are anticorrelated with pulses of activation of RpoS (8). However, it is not clear whether this feature is specific to RpoS or if it is common to many genes. We asked whether the pulsatile dynamics we observed coincided with dynamic patterns in growth rate. To test this, we extracted the instantaneous growth rate from cell lineages over time and compared them to fluorescence data for the different reporters. We observed distributions of growth rates that were similar across all reporters and strains used in this study (*SI Appendix*, Fig. S14).

In principle, fluorescence levels, which report underlying cellular properties such as those related to metabolism, can precede changes in growth (32). Alternatively, growth can drive changes in fluorescence since it affects dilution rates; regulatory links between growth rate and fluorescence are also possible (Fig. 3*A*). In both cases, these relationships could be positive or negative depending on the precise underlying mechanism.

To distinguish between these possibilities, we first computed temporal cross-correlations between fluorescence (F) and growth rate (μ), $R_{F,\mu}(\tau)$ (Fig. 3*B*). The cross-correlation measures how well the fluorescence and growth signals are correlated when the growth signal is shifted by a time τ relative to the fluorescence signal. Cross-correlation curves for our reporters have characteristic shapes, where signals are uncorrelated at large positive and negative values of the time shift, τ. For intermediate values of τ, we regularly observed valleys in the cross-correlation. We defined ($\tau_{extreme}$, $R_{extreme}$) as the coordinates of the point on the cross-correlation curve with the largest absolute value, indicating the largest correlation between the fluorescence and growth rate signals. $R_{extreme}$ can be either positive or negative, depending on whether the signals are correlated or anticorrelated. We also defined $\tau_{extreme}$ as the time shift associated with $R_{extreme}$, where $\tau_{extreme} < 0$ when changes in fluorescence precede changes in growth and $\tau_{extreme} > 0$ when growth leads fluorescence.

Growth and Expression Are Often Anticorrelated, with Growth Leading Expression. We found examples where a strong anticorrelation between fluorescence and growth were visible, such as with the *gadX* reporter, and other cases where the signals were uncorrelated, such as with the *recA* reporter (Fig. 3*C*). To quantify this trend across many cell lineages, we calculated cross-correlations between fluorescence and growth rate for all reporters (Fig. 3*D*). In many cases we observed an anticorrelation with a positive time shift between growth rate and gene expression, indicating that the pulses of expression from these promoters were preceded by a decrease in growth rate. In addition, we confirmed that the chromosomally integrated version of the *gadX* reporter produces cross-correlation curves that are similar to the plasmid-based version (*SI Appendix*, Fig. S15).

We found that changes in growth rate never lagged changes in fluorescence for all reporters we measured ($\tau_{extreme} > 0$) (*SI Appendix*, Fig. S16). It is possible that fluorophore maturation times could systematically introduce a lag between actual expression changes and read-out of the fluorescent protein. Maturation times for our reporters are relatively rapid, with 50% of fluorescent proteins maturing within ∼6 min (33); however, reporter maturation times could systematically introduce a modest positive shift in $\tau_{extreme}$. Overall, our measurements indicate that even cells growing exponentially under optimal conditions undergo episodes of slow growth that are largely followed by the pulses of stress-related genes, which frequently demonstrate an inverse relationship between growth rate and fluorescence.

Many of the genes in our library have long half-lives, and thus the relationship between the proteins they encode and growth rate may be similar to our experiments with stable fluorescent proteins. Examples of specific proteins include EvgA, RecA, and PhoP which have half-lives of 3 to 4 h (34). Although half-lives are not known for all proteins we considered, most proteins in *E. coli* are slowly degraded (35). Thus, delayed anticorrelations between growth and fluorescence signals are likely indicative of many of the protein concentration and growth rate relationships.

Promoter Activity Is Typically Positively Correlated with Growth. Accumulation of fluorescent proteins resulting from reduced dilution due to cell growth and division could potentially generate the delayed anticorrelation relationship we observed for many of the genes. However, we observed only a modest anticorrelation for several of the promoters, a near-zero or mildly positive relationship for the constitutive reporter, and no anticorrelation for *recA* and *sulA* (Fig. 3*D*). Thus, the anticorrelation is not an unavoidable consequence of dilution but is instead dependent on the specific relationship between gene expression and growth. Although the specific mechanisms that generate this effect will require further study, reporters with transcription rates that are decoupled from growth rate might produce delayed anticorrelations as a result of dilution effects, while transcription rates proportional to growth rate could cancel out this effect, resulting in flat cross-correlation curves. Indeed, Klumpp et al. showed that constitutive gene expression can be growth-rate-dependent, while expression of other genes is independent of growth rate (36).

In order to help decouple expression and growth rate effects, we also calculated promoter activity, which quantifies the rate of expression from the promoter. Promoter activity signals fluctuate over time and exhibit more rapid changes than the fluorescence signals (*SI Appendix*, Fig. S17*A*). We observed low or slightly anticorrelated relationships between cell growth and promoter activity for *gadX* and positive correlations for *recA*. We repeated the cross-correlation analysis for all reporters using the promoter activity signal and growth rate (*SI Appendix*, Fig. S17*B*). The promoter activity was often positively correlated with growth with no time shift between the two signals ($\tau_{extreme} \cong 0$) (*SI Appendix*, Fig. S17 *C–E*). We also observed instances of weak (e.g., *gadW* and *rob*) or mildly negative correlations (e.g., *gadX*). Together, these results suggest that the delayed anticorrelation in the cross-correlation between fluorescence and growth is largely due to cell dilution; however, the relationship between the rate of gene expression and growth varies widely across the reporters.

Gene Expression and Growth Dynamics Impact Single-Cell Survival under Stress. A critical question is whether these changes in gene expression and growth have concrete implications for whether a single cell will survive or die following stress. In other words, are the dynamics we observed sufficient to provide meaningful phenotypic differences that cause a cell to tolerate or succumb to stress? Slow growth and induction

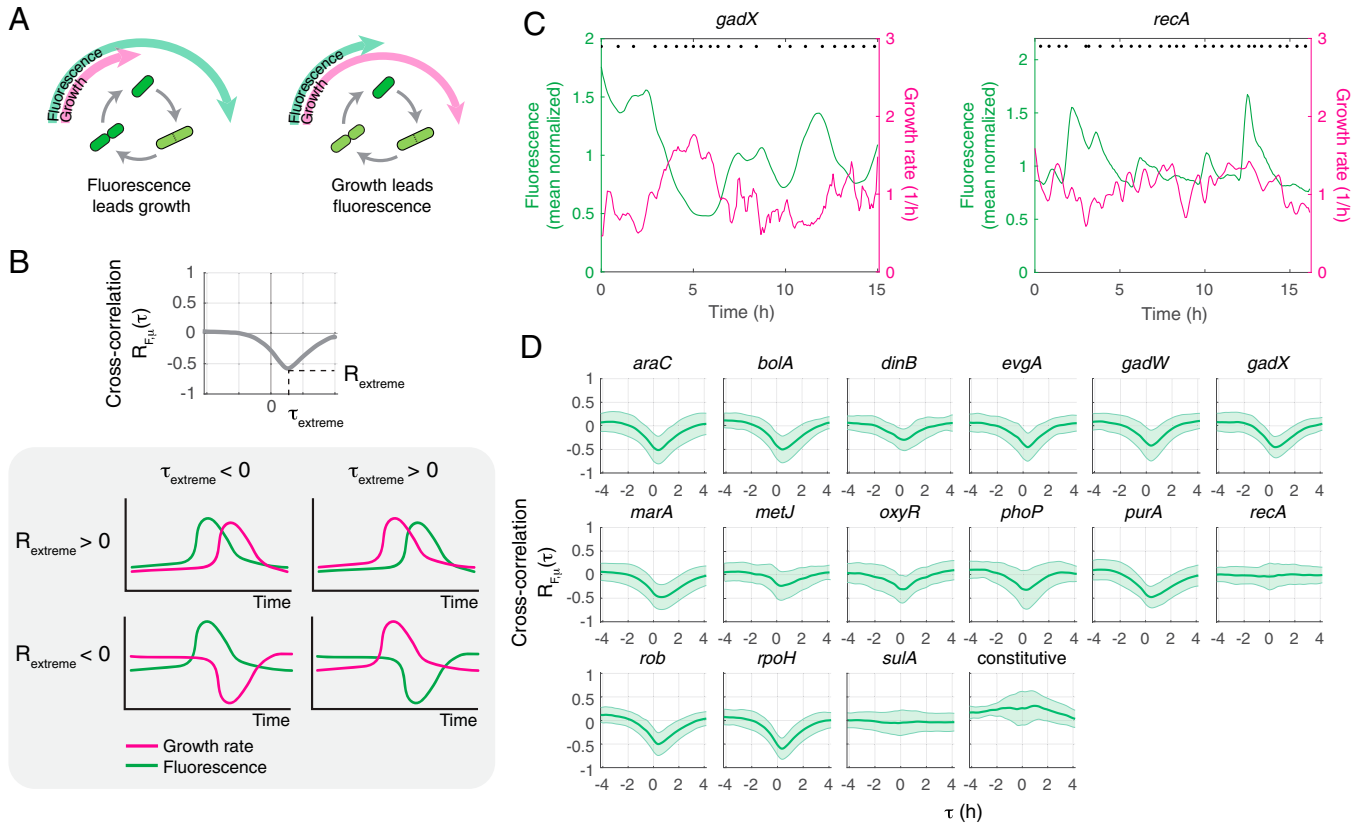

Fig. 3. Growth and gene expression dynamics are often anticorrelated. (*A*) Two possible models for the relationship between fluorescent reporter levels and growth. (*B*) Schematic of cross-correlation function between fluorescence (*F*) and growth rate (μ), $R_{F,\mu}(\tau)$ indicating points corresponding to $R_{extreme}$ and $\tau_{extreme}$ (*Top*). Temporal patterns of the fluorescence and growth rate and their impact on $R_{extreme}$ and $\tau_{extreme}$ (*Bottom*). (*C*) Representative fluorescence (green) and growth rate (magenta) values over time for a single mother cell with a reporter for *gadX* (*Left*) or *recA* (*Right*). Black dots at the top of the figure indicate cell division events. To aid visualization, growth rate data in this figure are smoothed with a moving average filter with a window of five frames in addition to the standard data processing described in *Materials and Methods*. (*D*) Cross-correlations between fluorescence and growth for all reporters. Shaded region represents SD about the mean.

of stress-response genes have previously been reported as mechanisms that allow survival at the populational level (37–41). This prompted us to investigate whether gene expression and growth dynamics influence the chances of survival under stress. Further, we asked whether survival was the result of a fortuitous condition of gene expression or slow growth upon stress introduction, or if a cell's past history was important.

For these studies, we first focused on expression of *gadX*, as our measurements demonstrate that this reporter is expressed in large pulses and has a strong anticorrelation with growth. In a prior study, we demonstrated that *gadX* is heterogeneously expressed in the absence of antibiotic stress and that expression levels correlate with longer survival times under constant carbenicillin and ciprofloxacin exposure (7). However, it was not clear how prior history or pulsing dynamics contribute to this phenotype and whether cells could recover normal cell division after transient drug treatment. Thus, we quantified how *gadX* and growth fluctuations preceding sudden exposure to a lethal antibiotic dose influence survival. We leveraged the mother-machine device to rapidly switch input media and exposed exponentially dividing cells to a short pulse of ciprofloxacin, a fluoroquinolone drug widely used to treat bacterial infections. We treated cells with 2 μg/mL ciprofloxacin, which corresponds to 100× the minimum inhibitory concentration, for 35 min before switching back to growth medium without antibiotic. This experimental setup allowed us to monitor the dynamics of *gadX* expression and growth in single cells prior to antibiotic stress while also recording the outcome of each cell lineage.

Within the same experiment, we observed instances where single cells were able to survive ciprofloxacin treatment (Fig. 4*A* and Movie S4) and cases where treatment killed the cells (Fig. 4*B* and Movie S5). In addition to surviving and dying, we also observed a third category of outcomes where cells filamented. However, it was difficult to accurately assess whether these cells survived or died, as they were frequently swept out of the mother-machine chamber and lost from the field of view. Thus, we focused our analysis on the surviving and dying cells because we could accurately determine their outcomes. By tracking gene expression history preceding antibiotic treatment, we observed pulses in fluorescence from the *gadX* reporter prior to ciprofloxacin addition in both the surviving and dying cells (Fig. 4*C*). Cells that exhibited expression pulses in the past, but had low expression at the time of ciprofloxacin treatment, were more likely to die. In contrast, cells which were in the fortuitous state of having an ongoing *gadX* pulse at the time of ciprofloxacin addition were more likely to exhibit transient stress tolerance.

We also looked at cellular outcome as a function of the growth rate. Consistent with our results showing anticorrelations between fluorescence and growth for *gadX* (Fig. 3*D*), we observed decreased growth rates in cells that survived, which were associated with increases in fluorescence signals (Fig. 4*D*). By looking at gene expression and growth rate history prior to ciprofloxacin addition, we see clear differences

emerging between the populations of cells that will survive and die starting ∼5 h prior to treatment (Fig. 4 *E* and *F*). The trend we observe does not reflect a linear increase in fluorescence in individual cells but rather results from *gadX* pulsing dynamics (Fig. 4 *C* and *E*). Similarly, decreases in growth rate accumulate based on contributions from individual cell dynamics (Fig. 4 *D* and *F*). For surviving and dying cohorts, we quantified how long each cell had been experiencing its final pulse of *gadX* expression at the point when ciprofloxacin was introduced (Fig. 4*G*). We found that a broad range of pulse lengths led to survival, while cells that died were rarely in an extended pulse.

Both Elevated Expression of Stress-Response Genes and Slow Cell Growth Contribute to Survival. Because growth rate and expression of stress-response genes are linked, a key question is whether survival is simply a by-product of slow growth, or if elevated gene expression and slow growth act synergistically. Disentangling this is challenging because growth, fluorescence, and survival are all correlated, but not necessarily causally related. To investigate this, we used a minimal model of causal inference to consider all possible impacts of growth and gene expression on survival. Conceptually, we considered three scenarios (Fig. 4*H*): growth rate (μ) and gene expression (reported by fluorescence, F) both impact survival; μ is linked with survival, but F has no impact; and F is linked to survival, but μ has no impact. These three possible relationships between μ, F, and survival can all be associated with correlations between fluorescence and survival, but the causal relationships are different in each case.

For example, the three scenarios will each produce different single-cell outcomes (survived or died) when fluorescence is plotted as a function of growth rate, even when μ and F are correlated in the same way (Fig. 4*I*). When both μ and F impact survival, the line that best separates the populations that survived and died will be diagonal. In contrast, when μ only impacts survival, the line is vertical. When F solely impacts survival, the line is horizontal. Importantly, these lines of separation represent where the probability of survival (P) is 0.5. Thus, it is not expected that all points that fall on one side of the line will be surviving cells and those on the other will die (this would imply a probability of 1 on one side and 0 on the other, rather than a smooth transition between these probabilities). Instead, the region where $P > 0.5$ is more likely to have cells that survive but will also contain some cells that die.

Inferring causal relationships is an intensive topic of study in statistical analysis (42–45). We employed a multiple regression, coupled with estimates of prior distributions, to predict the most likely causal relationships given our data. To quantify the causal contributions between μ and F with survival in the model (Fig. 4*H*), we defined parameters β_μ and β_F, where $\beta_\mu = 0$ or $\beta_F = 0$ indicate that μ or F do not contribute to survival, respectively. Positive values for these terms indicate complementary relationships and negative values indicate inverse relationships. In addition, the parameter γ quantifies the relationship between μ and F. Similarly, the model can infer that this relationship is not present, positive, or negative. The model is fit to the distributions of growth rate and fluorescence values that we observed experimentally (*SI Appendix*). Briefly, the model assumes a normal distribution for growth rates and a log-normal distribution for fluorescence values, which is a function of the value of μ. Survival is a binary variable, which we model using a Bernoulli distribution, with probability of survival determined as a function of the values of μ and F.

To generate simulated data on which to test performance of the minimal model for causal inference, we used a stochastic simulation of gene expression based on the random telegraph model (46–49). This stochastic mechanistic model accounts for promoter activity, transcription, and translation and includes a model for cell survival and death (*SI Appendix*). We generated data for each of the three scenarios: μ and F impact survival together, μ impacts survival alone, and F impacts survival alone. We used these simulated data points and plotted single-cell outcomes (survival or death) as a function of growth rate and fluorescence at the time of antibiotic addition (Fig. 4*J*). Using these data, we computed the likelihood of the minimal model parameters, including β_μ, β_F, and γ, to generate the posterior distribution (Fig. 4*K*). Feeding this posterior distribution into the minimal model in a forward fashion allowed us to compute the posterior predictive distribution of cell outcomes as a function of μ and F (Fig. 4*J*). We next used the model parameters to visualize the line representing a survival probability of 0.5.

The minimal model was able to correctly capture the causal relationships between μ, F, and survival from the stochastic simulation data. In the case where both μ and F have a direct impact on survival, both β_μ and β_F have nonnegligible values (Fig. 4*K*) and the line showing the 0.5 probability of survival is diagonal (Fig. 4*J*). When only μ influences survival, the maximum a posteriori of β_F is close to zero, and the 0.5 probability line is approximately vertical. Similarly, when only F influences survival, the maximum a posteriori of β_μ is close to zero, and the 0.5 probability line is approximately horizontal. Thus, the minimal model for causal inference can distinguish between alternative direct relationships between gene expression, growth, and survival.

Building upon the intuition from the stochastic simulation results, we next tested this approach on experimental data. Measurements for the *gadX* reporter of the instantaneous fluorescence and growth rate at $t = 0$, just prior to antibiotic addition, tend to show an inverse correlation between fluorescence and growth rate (Fig. 4*L*). For example, most surviving cells exhibited both elevated *gadX* expression and reduced growth rate immediately prior to ciprofloxacin treatment (Fig. 4 *C* and *D*). However, this correlation between growth rate and fluorescence does not imply causation. Thus, we next used these data to fit the values of the minimal model parameters, including β_μ, β_F, and γ, and computed the posterior predictive distribution of cell outcomes.

For the *gadX* reporter, we found that β_μ was negative, β_F was positive, and, correspondingly, the line representing the 0.5 survival probability was diagonal, indicating that both gene expression and growth impact survival (Fig. 4 *L* and *M*). The negative value of β_μ indicates that growth rate and survival are inversely related, as expected since slow growth is known to have a protective effect (2, 8, 18–20). Positive values of β_F indicate that higher levels of *gadX* expression directly influence survival. These relationships with survival characterized by negative values of β_μ and positive values of β_F emerge ∼5 h in advance, consistent with the extended duration of the *gadX* pulses (*SI Appendix*, Fig. S18).

To investigate whether the expression of other genes may also correlate with survival, we monitored the expression of two additional reporters under ciprofloxacin treatment (Fig. 4*L*). First, we measured the dynamics of the *bolA* reporter, an important stress-response gene controlled by RpoS whose expression has been found to be anticorrelated with growth rate (8). Cells that survived treatment were more likely to be in the midst of a transient period of slow growth and high *bolA* expression, while cells in the dying cohort were not (*SI Appendix*, Fig. S18). We also tracked the expression of *recA*,

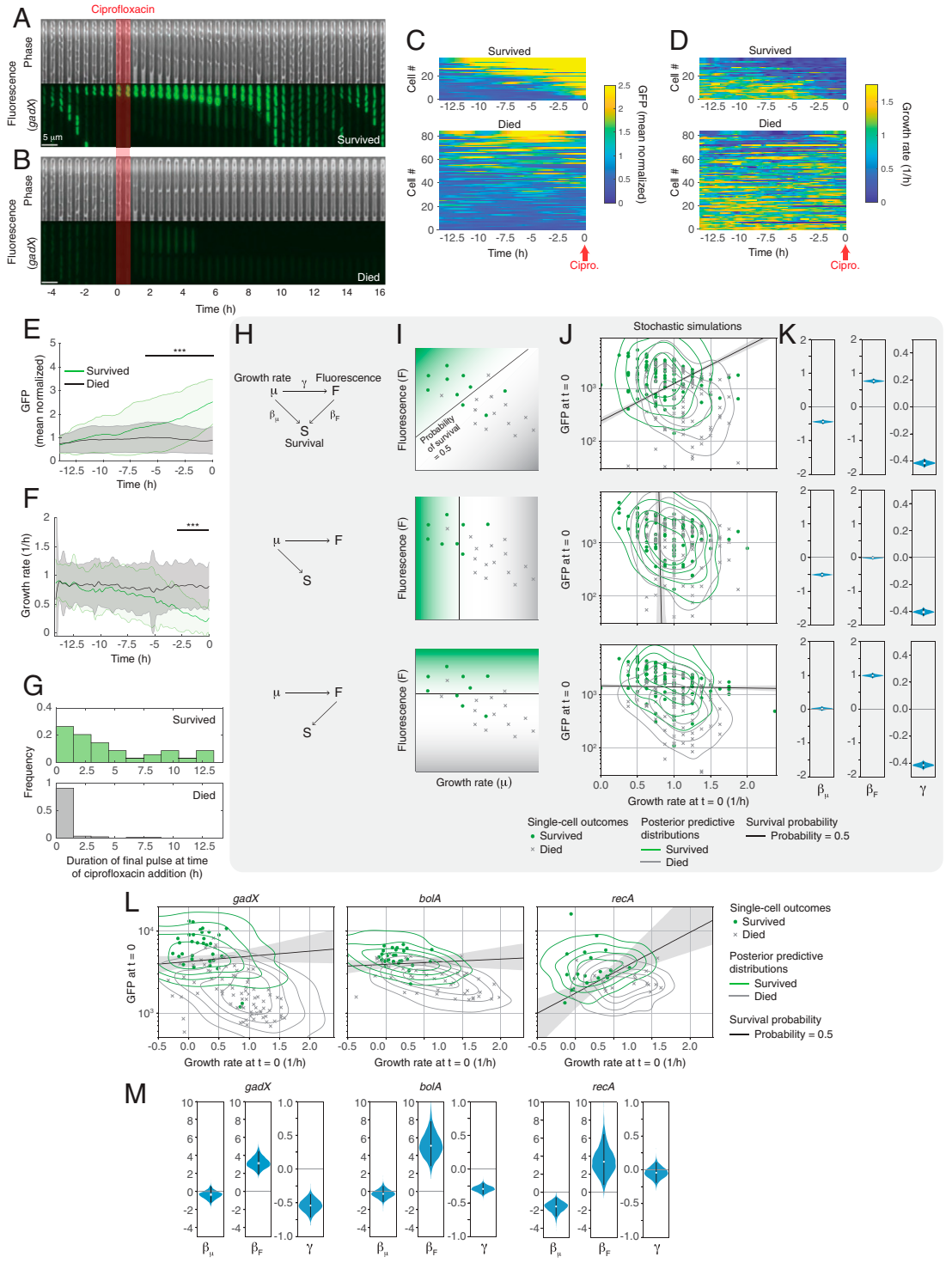

Fig. 4. Cell-to-cell differences in gene expression and growth influence survival outcomes after antibiotic exposure. (*A*) Representative kymograph of a cell lineage with *gadX* reporter that survives and (*B*) dies after antibiotic treatment. Images are from nearby chambers within the same microfluidic chip. Shaded area in red indicates 35-min period of ciprofloxacin treatment. (*C*) Single-cell *gadX* expression and (*D*) growth rate for the period preceding ciprofloxacin treatment. Cell numbers in *C* and *D* correspond to the same cells. Time series are sorted by the mean value of the fluorescence signal for t < 0, from high to low. (*E*) Mean fluorescence from the *gadX* reporter (*F*) and growth rate for the period preceding ciprofloxacin addition, with cells that survived or died separated. Shaded regions correspond to SD about the mean. Statistics are conducted at each time point; the horizontal bar indicates time points after which $P < 0.001$ (***), two-sample *t* test for differences between the mean of the cells that survived and died. (*G*) Histogram of duration of the pulse that cells were in upon ciprofloxacin addition, sorted by outcome. (*H*) Minimal model for causal relationships between growth rate (μ), gene expression (as reported by fluorescence, F), and survival and associated parameters. (*I*) Schematics showing data with identical correlations between μ and F but different causal relationships for survival. (*J*) Stochastic simulation results used to generate data that were then fit to the minimal model for causal inference. Gray shaded region shows the area where the probability of survival is between 0.9 and 0.1. Contour lines show the posterior predicted distributions from the fit to the minimal model. (*K*) Predicted values for β_μ, β_F, and γ from the data in *J*. Violin plots show the marginal posterior distribution of each of the three variables. The black lines show the 94% highest density interval (HDI), i.e., the smallest interval containing 94% of the probability. Each row in *I*–*K* corresponds to the scenario shown in that row in *H*. (*L*) Experimental data showing fluorescence values of individual cells carrying reporters for *gadX*, *bolA*, and *recA* that survived (green) or died (gray) following ciprofloxacin treatment plotted as a function of growth rate and fluorescence at t = 0. Gray shaded region and contour lines are as described in *J*. (*M*) Predicted values for β_μ, β_F, and γ from the *gadX*, *bolA*, and *recA* experimental data. Violin plots are as described in *K*.

which we selected because its fluorescence levels were not strongly correlated with growth rate (Fig. 3*D*). For both *bolA* and *recA*, the results mirror the effects observed for *gadX*, corroborating the important roles of both gene expression and slow growth in survival and suggesting the potential for collective protective impact of different proteins encoded by stress-response genes that accumulate during slow growth episodes. In addition, we compared the estimated values of γ, which describe the relationship between growth and fluorescence. The minimal model estimates negative values of γ for the *gadX* and *bolA* reporters and values for γ near zero for the *recA* reporter. These estimates are consistent with experimental results measured using cross correlations (Fig. 3*D*), demonstrating that the minimal model captures the essential features in the complex relationship between gene expression, growth, and survival.

Discussion

Although cells can display substantial phenotypic heterogeneity in constant environmental conditions, the timescales over which gene expression levels and growth rate fluctuate and how this ultimately impacts function are often less clear. To provide insight into these questions, we focused on genes involved in stress response in *E. coli*. Our results demonstrate that distributions of gene expression levels and growth rates can originate from rich dynamic activity, where individual cells transition between expression levels over time. Our findings expand previously published observations on pulsing dynamics (8, 13, 14, 17, 50) to a broader set of genes, suggesting that these time-varying differences in expression and growth may be more common than previously appreciated. These fluctuations occur under uniform, unstressed conditions and are observed across genes with diverse stress-response roles. Notably, temporal changes in gene expression are also related to growth. In our measurements, we found many instances where pulses of high activity followed decreases in growth rate. However, this link is not universal and is potentially indicative of differences in how gene expression rates are related to growth rate. Finally, we asked whether gene expression dynamics have functional consequences. We showed that a functional outcome of a decrease in growth rate is that cells are more likely to survive following sudden exposure to a lethal dose of ciprofloxacin. This coincides with increases in expression of several of the stress-response genes we measured in our study, where both slow growth and elevated gene expression work together to provide a synergistic protective effect.

Our results join a small number of other studies demonstrating examples of functional phenotypic heterogeneity. For example, the stochastic activation of diverse stress-response genes, such as those encoding porins (51), the catalase-peroxidase KatG (52), and the multiple antibiotic resistance activator MarA (6, 53, 54), result in transient tolerance to exogenous stress. Other examples include biased partitioning of efflux pumps during cell division that results in differential antibiotic susceptibility (55) and heterogeneous induction of *gad* regulon genes during antibiotic treatment that cross-protects cells against subsequent acid stress (9).

Reduced growth rates are known to enable cells to transiently resist stress, for example by playing a major role in the formation of persister cells (38, 56). By tracking expression dynamics and growth rates simultaneously, we found many instances in which these metrics are inversely correlated over time. Interestingly, an analogous observation was reported by Patange et al. (8) that demonstrated that the stress-response master regulator RpoS is expressed with pulsatile dynamics in exponentially dividing cells and is inversely correlated with growth rate. We demonstrated that RpoS availability directly influences pulsing dynamics in *gadX*, *evgA*, and *gadW* and could potentially serve as a common mechanism underlying the expression and growth dynamics associated with additional genes characterized in our study. Other mechanisms are also possible, as several genes in our study (e.g., *marA*) are not known to be regulated by RpoS. In some instances other mechanisms have been demonstrated, as in a recent study that indicated that self-degradation of the SOS response repressor LexA triggers pulses in the expression of *recA* and *sulA* during exponential growth in unperturbed conditions (14). Fluctuations in LexA result in frequent pulses in *recA* expression, while *sulA* is less susceptible to LexA variability, corroborating our observations. It is also noteworthy that, in addition to RpoS, at least one additional sigma factor, RpoH, was activated with pulsatile dynamics during exponential growth, a behavior that can potentially be propagated to >150 downstream genes that collectively control the cellular heat-shock response (57, 58). The pulsatile activity of these regulators might indicate that the mechanism by which sigma factors "time share" RNA polymerase complexes previously described in *B. subtilis* (59) might also be present in *E. coli*. Additionally, the pulses of activation of different sigma factors might be associated with different cellular growth statuses.

A link between the expression of genes in the *gad* regulon and survival to antimicrobial drugs has also been observed in other studies (7, 60). For example, overexpression of *gadX* can extend survival times under carbenicillin treatment (7). Our results provide important insights into potential additional mechanisms underlying this effect. We demonstrate that pulses of *gadX* expression coincide with episodes of slow growth, which can contribute to survival. Additionally, many stress-response genes display pulsatile expression dynamics and anticorrelation with growth rate, and we show that elevated expression and slow growth in both *bolA* and *recA* are also linked to a higher likelihood of survival. Additionally, our minimal model results suggests that both elevated gene expression and reduced growth rate play a causal role in protecting cells from antibiotic stress. The collective accumulation of stress-response proteins may serve to amplify the tolerance of single cells undergoing periods of slow growth.

In future experiments, it would be interesting to conduct measurements using pairs of reporters so that expression pulses can be monitored simultaneously in the same cell. This is particularly interesting to examine in relation to the growth rate, as we observed many instances of anticorrelation, but the temporal properties of these pulses were distinct from each other. Although we measure growth rate in our analysis, our findings do not preclude the possibility that growth rate is a secondary effect that is downstream of the true coordinating signal, such as metabolic state (32, 61). Experiments that use reporters to measure genes involved in metabolism alongside the stress-response reporters or studies that carefully control the nutrient composition could be used to investigate this possibility. It will also be interesting to investigate how the information encoded in transcription factor dynamics is transmitted to downstream genes, and emerging technologies that enable the manipulation of gene expression over time could help to identify how these signals are propagated (62, 63). Finally, although we have focused our analysis of stress survival on transient ciprofloxacin treatment in wild-type cells, it would be interesting to test survival in other antibiotics, different stress application patterns, and the effect of different strain backgrounds.

In summary, our findings reveal that pulsatile dynamics in gene expression and growth serve as a mechanism that cells can leverage

to transiently resist stress. This dynamic behavior is spread across a broad range of stress-response genes, including heat-shock response, multidrug resistance, and oxidative stress and can enable subpopulations of cells to withstand temporary stress.

Materials and Methods

Strains and Growth Media. Strains containing reporter plasmids were sourced from the collection created by Zaslaver et al. (64), unless otherwise noted. Briefly, each strain has a low-copy-number plasmid (SC101 origin) containing the promoter sequence for the gene of interest upstream of the coding sequence for *gfpmut2* green fluorescent protein (GFP). Further details on plasmid and strain construction are provided in *SI Appendix*.

Cells were grown in M9 medium (0.1 mM $CaCl_2$, 2 mM $MgSO_4$, and 1× M9 salts) supplemented with 0.4% glucose, 0.2% casamino acids, and 30 μg/mL kanamycin for plasmid maintenance. Media used in microfluidic experiments were supplemented with 2 g/L F-127 Pluronic to prevent cell adhesion and growth outside of the mother-machine growth chambers.

Static Fluorescence Microscopy Snapshots. Overnight cultures were diluted 1:100 and incubated at 37 °C with shaking for 2.5 to 4 h (optical density at 600 nm [OD_{600nm}] = 0.7 to 1.3). One microliter of cells was placed on 1.5% MGC (0.2% glycerol, 0.01% casamino acids, 0.15 μg/mL biotin, and 1.5 μM thiamine) low-melting-point agarose pads and imaged at 100× on a Nikon Ti-E inverted fluorescence microscope. Three separate overnight cultures were sampled and imaged for each reporter strain.

Mother-Machine Microfluidic Device. The mother-machine microfluidic master mold used was described previously in ref. 26. Briefly, the master mold chip has eight independent main feed channels where growth media flows in and out. Each channel features 1,000 one-ended chambers (length × width × height = 25 μm × 1.3 μm × 1.1 μm) where the mother cells are trapped. We made the microfluidic devices by pouring a degassed 10:1 mixture of dimethylsiloxane monomer and curing agent (Sylgard 184 Silicone Elastomer Kit; Dow Corning) onto the wafer, which was then cured overnight at 65 °C. Individual chips were separated from the mold and a 0.75-mm biopsy punch was used to create inlets and outlets for each flow channel before the chip was plasma bonded to a glass slide.

Time-Lapse Microscopy Movies. Overnight cultures were diluted 1:100 and incubated at 37 °C with shaking for ∼3 h until midexponential phase (OD_{600nm} = 1.0–1.3). Cells were concentrated by centrifugation (6,000 × *g* for 2 min) and loaded into the microfluidic chip. Cells were seeded in the growth chambers by centrifugation at 6,000 × *g* for 3 min. Media was supplied at a flow rate of 20 μL/min using a peristaltic pump. Cells were allowed to adapt to growth in the device for 2 to 4 h before imaging. Time-lapse movies were acquired with a 100× oil objective on a Nikon Ti-E inverted fluorescence microscope equipped with a perfect focus system and a temperature control chamber that was set at 37 °C for the duration of the experiment. Images were acquired in phase contrast and epifluorescence illumination with a green or cyan fluorescent protein filter every 5 min. The total number of cell lineages tracked for each reporter is listed in *SI Appendix*, Table S3.

Microscopy Image Processing and Fluorescence and Growth Rate Analysis. For static snapshots, cell images were segmented with the SuperSegger software (65). For mother-machine experiments, we performed automated cell segmentation and lineage tracking using the deep learning-based software DeLTA (26). In both cases, reported single-cell fluorescence values are the average fluorescence intensities of all pixels belonging to each cell. Unless otherwise noted, for mother-machine experiments only data for the "mother" cell trapped at the top of the growth chambers was used in quantitative analysis. We smoothed the fluorescence data using a moving average filter with a window of five frames.

To estimate growth rates, we calculated the difference in cell length between adjacent frames normalized by the cell length, $1/L\ dL/dt$. Specifically, when there is no cell division event between frames, this is calculated as $\ln(L_{i+1}/L_{i-1})/(2\Delta t)$, where L_i is the length of the cell at time t_i, L_{i-1} is the length at the preceding frame, L_{i+1} is the length at the subsequent frame, and Δt is the time between frames (5 min = 0.083 h). In cases where a cell division event occurs, this calculation is modified to $\ln([L_{i+1} + D_{i+1}]/L_{i-1})/(2\Delta t)$, where D_{i+1} is the length of the daughter at time t_{i+1}. After calculating the growth rate, we smoothed the data using a moving average filter with a window of five frames.

Cell division times are calculated as the time between division events.

Pulse Identification. To allow comparison across all reporters, which have different expression levels and where imaging exposure times are different (*SI Appendix*, Table S3), we normalized each time series by its mean. Pulses of gene expression were identified using the built-in MATLAB function *findpeaks*, which identifies local maxima. We set the threshold for the minimum peak prominence at 0.5, unless otherwise noted. This value was determined empirically (*SI Appendix*, Fig. S9).

Promoter Activity Calculations. Promoter activity was calculated as in Patange et al. (8) as $M\left(\frac{1}{L}\frac{dL}{dt} + \lambda_p\right) + \frac{dM}{dt}$, where M is the cell's average fluorescence value, L is the cell length, $\lambda_p = 0.1$, and postprocessing is applied to remove spurious negative values of $\frac{dL}{dt}$.

Autocorrelation and Cross-Correlation Calculations. We calculated the autocorrelation of the fluorescence signal–$R_{F,F}(\tau)$ where τ is the time shift–using the MATLAB function *xcov* with the "normalized" method. The half-life was calculated by taking the mean of all autocorrelation signals from individual cell lineages and identifying the time shift value where it crosses 0.5.

The cross-correlation between the fluorescence signal and the growth rate, $R_{F,\mu}(\tau)$, was calculated using the MATLAB function *xcov* with the "normalized" method. $R_{PA,\mu}(\tau)$ was calculated with the same approach, but with the promoter activity and growth rate.

$R_{extreme}$ is the value of $R_{F,\mu}(\tau)$ with the largest absolute value. $\tau_{extreme}$ is the time lag value associated with $R_{extreme}$.

Antibiotic Survival Assay. Mother-machine experiments were initiated using the methods described above. During image acquisition, cells were provided with fresh medium for at least 10 h, followed by 35 min of treatment with medium supplemented with 2 μg/mL ciprofloxacin, then fresh medium again for 16 h. The outcomes of ciprofloxacin treatment for each lineage were manually scored as "survived," "died," or "filamented." Cells were scored as "survived" if cell division was observed in the chamber at the end of the full 16 h after the second addition of fresh medium. Cells were scored as "died" if growth permanently ceased in the chamber at any point after antibiotic exposure. "Filamented" cells were excluded from the analysis, as it was difficult to accurately assess their outcome since they were frequently swept out of the chamber and field of view.

Causal Influence Model. The causal influence model is composed of three interacting variables: the growth rate (μ), fluorescence (F), and survival (S). S is a binary variable representing the cell outcome (survived or died). The model assumes that fluorescence cannot causally influence growth rate because we found experimentally that changes in fluorescence never precede changes in growth rate for any reporter, but μ and F may influence survival and μ may influence F. The growth rate is assumed to be at steady state and distributed according to a normal distribution. The fluorescence is assumed to be distributed according to a log-normal distribution. The average of the underlying normal distribution is assumed to be linearly related to the growth rate, while its variance is fixed, which is consistent with the experimental data. Finally, the survival outcome is treated as resulting from a weighted Bernoulli distribution (coin flip) with a probability of survival based on a logistic function acting upon a linear combination of growth rate and the logarithm of fluorescence: $\text{logit}(p_{survival}) = \alpha + \beta_\mu \mu + \beta_F F$. Statistical inference was performed with PyMC3 (66), a Python package for probabilistic programming. Full details of the model, including a description of the parameters α, β_μ, β_F, and γ, are provided in *SI Appendix*.

Stochastic Simulations. The stochastic model is an extension of the random telegraph model (46–49). To model bursts of gene expression, it simulates random activations and deactivations of a promoter, transcription when the promoter is activated, translation, and degradation of both messenger RNA and proteins. We extended this model in two ways: including a stochastic growth rate and cell division model, and a model of death caused by antibiotics. The model was implemented in Rust with the Gillespie algorithm (67). Full details of the model are provided in *SI Appendix*.

Data Availability. The processing algorithms for all data analysis and models conducted in this study are available in Gitlab at https://gitlab.com/dunloplab/sampaio-single-cell-gene-expression-and-growth. Single-cell microscopy data for gene expression and growth rate have been deposited in Zenodo (DOI: 10.5281/zenodo.6369878) (68) .

ACKNOWLEDGMENTS. We thank members of the M.J.D. laboratory and Wilson Wong for helpful discussions. Ahmad (Mo) Khalil and Razan Alnahhas provided input on the manuscript. Razan Alnahhas and Eric South conducted initial experiments with the constitutive reporter. This work was supported by NIH Grants R01AI102922 and R21AI137843. C.M.B. received support from the NSF Graduate Research Fellowship under Grant DGE-1840990.

Author affiliations: [a]Biomedical Engineering Department, Boston University, Boston, MA 02215; and [b]Biological Design Center, Boston University, Boston, MA 02215

1. Y. Taniguchi *et al.*, Quantifying *E. coli* proteome and transcriptome with single-molecule sensitivity in single cells. *Science* **329**, 533–538 (2010).
2. D. J. Kiviet *et al.*, Stochasticity of metabolism and growth at the single-cell level. *Nature* **514**, 376–379 (2014).
3. O. K. Silander *et al.*, A genome-wide analysis of promoter-mediated phenotypic noise in *Escherichia coli*. *PLoS Genet.* **8**, e1002443 (2012).
4. A. Raj, A. van Oudenaarden, Nature, nurture, or chance: Stochastic gene expression and its consequences. *Cell* **135**, 216–226 (2008).
5. A. Bar-Even *et al.*, Noise in protein expression scales with natural protein abundance. *Nat. Genet.* **38**, 636–643 (2006).
6. I. El Meouche, Y. Siu, M. J. Dunlop, Stochastic expression of a multiple antibiotic resistance activator confers transient resistance in single cells. *Sci. Rep.* **6**, 1–9 (2016).
7. N. A. Rossi, I. El Meouche, M. J. Dunlop, Forecasting cell fate during antibiotic exposure using stochastic gene expression. *Commun. Biol.* **2**, 1–7 (2019).
8. O. Patange *et al.*, *Escherichia coli* can survive stress by noisy growth modulation. *Nat. Commun.* **9**, 1–11(2018).
9. K. Mitosch, G. Rieckh, T. Bollenbach, Noisy response to antibiotic stress predicts subsequent single-cell survival in an acidic environment. *Cell Syst.* **4**, 393–403 (2017).
10. S. Uphoff *et al.*, Stochastic activation of a DNA damage response causes cell-to-cell mutation rate variation. *Science* **351**, 1094–1097 (2016).
11. S. Uphoff, Real-time dynamics of mutagenesis reveal the chronology of DNA repair and damage tolerance responses in single cells. *Proc. Natl. Acad. Sci. U.S.A.* **115**, E6516–E6525 (2018).
12. I. El Meouche, M. J. Dunlop, Heterogeneity in efflux pump expression predisposes antibiotic-resistant cells to mutation. *Science* **362**, 686–690 (2018).
13. J. H. Levine, Y. Lin, M. B. Elowitz, Functional roles of pulsing in genetic circuits. *Science* **342**, 1193–1200 (2013).
14. E. C. Jones, S. Uphoff, Single-molecule imaging of LexA degradation in *Escherichia coli* elucidates regulatory mechanisms and heterogeneity of the SOS response. *Nat. Microbiol.* **6**, 981–990 (2021).
15. G. M. Süel, R. P. Kulkarni, J. Dworkin, J. Garcia-Ojalvo, M. B. Elowitz, Tunability and noise dependence in differentiation dynamics. *Science* **315**, 1716–1719 (2007).
16. H. Maamar, A. Raj, D. Dubnau, Noise in gene expression determines cell fate in Bacillus subtilis. *Science* **317**, 526–529 (2007).
17. J. M. Kim, M. Garcia-Alcala, E. Balleza, P. Cluzel, Stochastic transcriptional pulses orchestrate flagellar biosynthesis in *Escherichia coli*. *Sci. Adv.* **6**, eaax0947 (2020).
18. M. M. Logsdon, B. B. Aldridge, Stable regulation of cell cycle events in mycobacteria: Insights from inherently heterogeneous bacterial populations. *Front. Microbiol.* **9**, 514 (2018).
19. Y. Tanouchi *et al.*, A noisy linear map underlies oscillations in cell size and gene expression in bacteria. *Nature* **523**, 357–360 (2015).
20. E. Biselli, S. J. Schink, U. Gerland, Slower growth of *Escherichia coli* leads to longer survival in carbon starvation due to a decrease in the maintenance rate. *Mol. Syst. Biol.* **16**, e9478 (2020).
21. D. A. F. Fuentes, P. Manfredi, U. Jenal, M. Zampieri, Pareto optimality between growth-rate and lag-time couples metabolic noise to phenotypic heterogeneity in *Escherichia coli*. *Nat. Commun.* **12**, 1–12 (2021).
22. J. Narula *et al.*, Slowdown of growth controls cellular differentiation. *Mol. Syst. Biol.* **12**, 871 (2016).
23. B. B. Aldridge *et al.*, Asymmetry and aging of mycobacterial cells lead to variable growth and antibiotic susceptibility. *Science* **335**, 100–104 (2012).
24. A. J. Lee *et al.*, Robust, linear correlations between growth rates and β-lactam-mediated lysis rates. *Proc. Natl. Acad. Sci. U.S.A.* **115**, 4069–4074 (2018).
25. P. Wang *et al.*, Robust growth of *Escherichia coli*. *Curr. Biol.* **20**, 1099–1103 (2010).
26. J. B. Lugagne, H. Lin, M. J. Dunlop, DeLTA: Automated cell segmentation, tracking, and lineage reconstruction using deep learning. *PLoS Comput. Biol.* **16**, e1007673 (2020).
27. A. Mukherjee, C. Cao, J. Lutkenhaus, Inhibition of FtsZ polymerization by SulA, an inhibitor of septation in *Escherichia coli*. *Proc. Natl. Acad. Sci. U.S.A.* **95**, 2885–2890 (1998).
28. O. Huisman, R. D'Ari, S. Gottesman, Cell-division control in *Escherichia coli*: Specific induction of the SOS function SfiA protein is sufficient to block septation. *Proc. Natl. Acad. Sci. U.S.A.* **81**, 4490–4494 (1984).
29. J. Bos *et al.*, Emergence of antibiotic resistance from multinucleated bacterial filaments. *Proc. Natl. Acad. Sci. U.S.A.* **112**, 178–183 (2015).
30. A. Tramonti, P. Visca, M. De Canio, M. Falconi, D. De Biase, Functional characterization and regulation of gadX, a gene encoding an AraC/XylS-like transcriptional activator of the *Escherichia coli* glutamic acid decarboxylase system. *J. Bacteriol.* **184**, 2603–2613 (2002).
31. S. W. Seo, D. Kim, E. J. O'Brien, R. Szubin, B. O. Palsson, Decoding genome-wide GadEWX-transcriptional regulatory networks reveals multifaceted cellular responses to acid stress in *Escherichia coli*. *Nat. Commun.* **6**, 7970 (2015).
32. P. Thomas, G. Terradot, V. Danos, A. Y. Weiße, Sources, propagation and consequences of stochasticity in cellular growth. *Nat. Commun.* **9**, 1–11 (2018).
33. E. Balleza, J. M. Kim, P. Cluzel, Systematic characterization of maturation time of fluorescent proteins in living cells. *Nat. Methods* **15**, 47–51 (2018).
34. N. Nagar *et al.*, Harnessing machine learning to unravel protein degradation in *Escherichia coli*. *mSystems* **6**, e01296-20 (2021).
35. M. R. Maurizi, Proteases and protein degradation in *Escherichia coli*. *Experientia* **48**, 178–201 (1992).
36. S. Klumpp, Z. Zhang, T. Hwa, Growth rate-dependent global effects on gene expression in bacteria. *Cell* **139**, 1366–1375 (2009)
37. E. Tuomanen, R. Cozens, W. Tosch, O. Zak, A. Tomasz, The rate of killing of *Escherichia coli* by β-lactam antibiotics is strictly proportional to the rate of bacterial growth. *J. Gen. Microbiol.* **132**, 1297–1304 (1986).
38. M. H. Pontes, E. A. Groisman, Slow growth determines nonheritable antibiotic resistance in *Salmonella enterica*. *Sci. Signal.* **12**, 1–11 (2019).
39. D. J. Evans, D. G. Allison, M. R. W. Brown, P. Gilbert, Susceptibility of *Pseudomonas aeruginosa* and *Escherichia coli* biofilms towards ciprofloxacin: Effect of specific growth rate. *J. Antimicrob. Chemother.* **27**, 177–184 (1991).
40. I. Yelin, R. Kishony, Antibiotic resistance. *Cell* **172**, 1136–1136 (2018).
41. A. C. Palmer, R. Kishony, Opposing effects of target overexpression reveal drug mechanisms. *Nat. Commun.* **5**, 4296 (2015).
42. L. Yao *et al.*, A survey on causal inference. *ACM Trans. Knowl. Discov. Data* **15**, 1–46 (2021).
43. J. Pearl, *Causality: Models, Reasoning, and Inference* (Cambridge University Press, ed. 2, 2011).
44. M. Eichler, Causal inference with multiple time series: Principles and problems. *Philos. Trans.-Royal Soc., Math. Phys. Eng. Sci.* **371**, 20110613 (2013).
45. R. McElreath, *Statistical Rethinking: A Bayesian Course with Examples in R and Stan* (CRC Press, ed. 2, 2020).
46. N. Kumar, A. Singh, R. V. Kulkarni, Transcriptional bursting in gene expression: Analytical results for general stochastic models. *PLoS Comput. Biol.* **11**, e1004292 (2015).
47. J. Peccoud, B. Ycart, Markovian modeling of gene-product synthesis. *Theor. Popul. Biol.* **48**, 222–234 (1995).
48. V. Shahrezaei, P. S. Swain, Analytical distributions for stochastic gene expression. *Proc. Natl. Acad. Sci. U.S.A.* **105**, 17256–17261 (2008).
49. M. Dobrzyński, F. J. Bruggeman, Elongation dynamics shape bursty transcription and translation. *Proc. Natl. Acad. Sci. U.S.A.* **106**, 2583–2588 (2009).
50. J. E. Purvis, G. Lahav, Encoding and decoding cellular information through signaling dynamics. *Cell* **152**, 945–956 (2013).
51. M. A. Sánchez-Romero, J. Casadesús, Contribution of phenotypic heterogeneity to adaptive antibiotic resistance. *Proc. Natl. Acad. Sci. U.S.A.* **111**, 355–360 (2014).
52. Y. Wakamoto *et al.*, Dynamic persistence of antibiotic-stressed mycobacteria. *Science* **339**, 91–95 (2013).
53. N. A. Rossi, M. J. Dunlop, Customized regulation of diverse stress response genes by the multiple antibiotic resistance activator MarA. *PLoS Comput. Biol.* **13**, e1005310 (2017).
54. J. Garcia-Bernardo, M. J. Dunlop, Tunable stochastic pulsing in the *Escherichia coli* multiple antibiotic resistance network from interlinked positive and negative feedback loops. *PLoS Comput. Biol.* **9**, e1003229 (2013).
55. T. Bergmiller *et al.*, Biased partitioning of the multidrug efflux pump AcrAB-TolC underlies long-lived phenotypic heterogeneity. *Science* **356**, 311–315 (2017).
56. N. Q. Balaban, J. Merrin, R. Chait, L. Kowalik, S. Leibler, Bacterial persistence as a phenotypic switch. *Science* **305**, 1622–1625 (2004).
57. F. Arsène, T. Tomoyasu, B. Bukau, The heat shock response of *Escherichia coli*. *Int. J. Food Microbiol.* **55**, 3–9 (2000).
58. T. Yura, Regulation of the heat shock response in Escherichia coli: History and perspectives. *Genes Genet. Syst.* **94**, 103–108 (2019).
59. J. Park *et al.*, Molecular time sharing through dynamic pulsing in single cells. *Cell Syst.* **6**, 216–229 (2018).
60. K. Mitosch, G. Rieckh, T. Bollenbach, Noisy response to antibiotic stress predicts subsequent single-cell survival in an acidic environment. *Cell Syst.* **4**, 393–403 (2017).
61. A. J. Lopatkin *et al.*, Bacterial metabolic state more accurately predicts antibiotic lethality than growth rate. *Nat. Microbiol.* **4**, 2109–2117 (2019).
62. J. B. Lugagne, M. J. Dunlop, Cell-machine interfaces for characterizing gene regulatory network dynamics. *Curr. Opin. Syst. Biol.* **14**, 1–8 (2019).
63. N. M. V. Sampaio, M. J. Dunlop, Functional roles of microbial cell-to-cell heterogeneity and emerging technologies for analysis and control. *Curr. Opin. Microbiol.* **57**, 87–94 (2020).
64. A. Zaslaver *et al.*, A comprehensive library of fluorescent transcriptional reporters for *Escherichia coli*. *Nat. Methods* **3**, 623–628 (2006).
65. S. Stylianidou, C. Brennan, S. B. Nissen, N. J. Kuwada, P. A. Wiggins, SuperSegger: Robust image segmentation, analysis and lineage tracking of bacterial cells. *Mol. Microbiol.* **102**, 690–700 (2016).
66. J. Salvatier, T. V. Wiecki, C. Fonnesbeck, Probabilistic programming in Python using PyMC3. *PeerJ Comput. Sci.* **2016**, e55 (2016).
67. D. T. Gillespie, Exact stochastic simulation of coupled chemical reactions. *J. Phys. Chem.* **81**, 2340–2361 (1977).
68. N. M. V. Sampaio, C. M. Blassick, V. Andreani, J.-B. Lugagne, M. J. Dunlop, Dynamic gene expression and growth underlie cell-to-cell heterogeneity in *Escherichia coli* stress response. Zenodo. 10.5281/zenodo.6369878. Deposited 16 March 2022.